

Association of the 3:2 HFQPO Pairs with the Broad Fe K Line in XTE J1550-564 and GRO J1655-40

Ding-Xiong WANG^{1,2}, Zhao-Ming GAN¹, Chang-Yin HUANG¹ and Yang LI¹

¹ Department of Physics, Huazhong University of Science and Technology, Wuhan, 430074, China

² Send offprint requests to: D.-X. Wang(dxwang@hust.edu.cn)

1 December 2018

ABSTRACT

Association of the high-frequency quasi-periodic oscillation (HFQPO) pairs with the broad Fe K line in XTE J1550-564 and GRO J1655-40 is discussed based on the magnetic coupling (MC) of a rotating black hole (BH) with its surrounding disc. The 3:2 HFQPO pairs are interpreted by virtue of the inner and outer hotspots arising from non-axisymmetric magnetic field, where the inner hotspot is produced by a torque exerted at the inner edge of the disc, and the outer hotspot is created by the screw instability of the large-scale magnetic field. The very steep emissivity index is created predominantly by the torque exerted at the inner edge of the disc. It turns out that the 3:2 HFQPO pairs observed in the two sources can be fitted by tuning several model parameters, such as the BH spin, and the main features of this model lie in three aspects. (1) The condition for only one HFQPO is discussed based on the two mechanisms for producing the 3:2 HFQPO pairs, (2) an explanation is given for a systematic shift away from disc dominated flux with the increasing power-law flux as the HFQPO pairs shift from the higher to lower frequencies, which is consistent with the analysis given by Remillard et al. (2002), and (3) the BH spin in XTE J1550-564 and GRO J1655-40 can be estimated by combining the 3:2 HFQPO pairs with the very steep emissivity index required for fitting the broad Fe K emission line.

Key words: accretion, accretion discs — black hole physics — magnetic fields — stars: individual (XTE J1550-564, GRO J1655-40) — stars: oscillations — X-rays: stars

1 INTRODUCTION

Quasi-periodic oscillations in black hole X-ray binaries (BHXBs) have become a very active research field since the launch of the NASA satellite *RXTE* (Bradt et al. 1993). One of the remarkable features in BHXBs is that the high-frequency quasi-periodic oscillations (HFQPOs) could appear in pairs with the puzzling commensurate frequencies, which have been observed in GRO J1655-40 (450, 300Hz; Remillard et al. 1999; Strohmayer 2001a; Remillard et al. 2002, hereafter R02), XTE J1550-564 (276, 184, 92Hz; Miller et al. 2001; R02) and GRS 1915+105 (168, 113, 67, 41Hz; McClintock & Remillard 2006; Remillard & McClintock 2006, hereafter MR06 and RM06, respectively). The above HFQPOs appear in pairs with the 3:2 ratio of the higher frequency to the lower frequency (henceforth 3:2 HFQPO pairs), e.g. 276 vs 184Hz and 450 vs 300Hz occur in XTE J1550-564 and GRO J1655-40, respectively, while two 3:2 HFQPO pairs, 168 vs 113Hz and 67 vs 41Hz, appear in GRS 1915+105.

A number of models have been proposed to explain the origin of HFQPO pairs in BHXBs. Strohmayer (2001a, 2001b) investigated combinations of the azimuthal and radial coordinate frequencies in general relativity to explain the HFQPO pairs in GRO J1655-40 and GRS 1915+105. Wagoner et al. (2001) regarded the HFQPO pairs as fundamental g-mode and c-mode discoseismic oscillations in a relativistic accretion disc. Very recently, Silbergleit & Wagoner (2007) discussed the corotation resonance and diskoseismology modes of black hole (BH) accretion discs and suggested that the HFQPO pairs may relate to the excitation of two (groups of) g-modes of discoseismic oscillations. Abramowicz & Kluzniak (2001) explained the pairs in GRO J1655-40 as a resonance between orbital and epicyclic motion of accreting matter. Recently, the resonance model is presented in a more realistic context, in which "parametric resonance" concept is introduced to describe the oscillations rooted in fluid flow where there is a coupling between the radial and polar coordinate frequencies (Abramowicz et al. 2003; Kluzniak et al. 2004; Török et al. 2005). As argued by van der Klis (2000, 2006), HFQPOs in X-ray binaries probably originate from

the inner edge of an accretion disc around a neutron star or a stellar-mass BH, since millisecond is the natural timescale for accretion process in these regions.

On the other hand, Wilms et al. (2001) presented the first XMM-Newton observation of MCG-6-30-15, and they found a broad Fe disc line from the observed spectrum. However, no quasi-periodic oscillations have been detected in this source. A very steep emissivity index ($4.3 < \beta < 5.0$) from the inner accretion disc is required for fitting the broad Fe K emission line, which is difficult to be explained within the framework of a standard accretion disc (SAD). Wilms et al. (2001) suggested that the magnetic extraction of rotational energy from a spinning black hole should be invoked to create this steep emissivity.

The relativistic disc lines for microquasars have been analyzed by some authors, e.g., XTE J1550-564 by Sobczak et al. (2000), Miller et al. (2003, 2004); XTE J1650-500 by Miller et al. (2004), Miniutti, Fabian, and Miller (2004); GRO J1655-40 by Miller et al. (2004), Diaz Trigo et al. (2007). However, the steep emissivity indexes required by broad Fe K α lines were hardly worked out except a few cases, such as, $\beta = 5.5_{-0.7}^{+0.5}$ for GX 339-4 in the very high state, and $\beta \simeq 5$ for XTE J1650-500 based on the observation of XMM-Newton. A detailed review for relativistic X-ray emission lines from the inner accretion disc around black holes for AGNs and stellar-mass black holes are given by Miller (2007).

With the existence of a magnetic field connecting a rotating black hole to its surrounding disc, energy and angular momentum can be transferred from the black hole to the disc, and this energy mechanism is referred to as the MC process, which is regarded as one of the variants of the Blandford-Znajek (BZ) process (Blandford & Znajek 1977, 1999; Li 2000, 2002, hereafter L02, Wang 2002).

Wang et al. (2002, 2003a, hereafter W03a) incorporated the BZ and MC processes into black hole accretion disc, and henceforth this model is referred to as MC-I model, which was used to interpret the very steep emissivity index required by the observation of MCG-6-30-15. In addition, Wang et al. (2005, hereafter W05) suggested that the 3:2 HFQPO pairs observed in the above BHXBs can be fitted by virtue of two hotspots in the inner disc, which are produced by the non-axisymmetric MC process.

The fatal shortcoming of MC-I model is that the fits of the 3:2 HFQPO pairs always accompany jets, which is driven by the BZ process. As reviewed in MR06 and RM06, jets are generally observed in the hard state of BHXBs, while HFQPOs are always detected in the steep power-law (SPL) state. Thus the fits of the 3:2 HFQPO pairs based on MC-I model are inconsistent with the observations.

Based on a careful analysis of the 1998-1999 outburst of XTE J1550-564 and the 1996-1997 outburst of GRO J1655-40 some interesting features have been found in R02, the 3:2 HFQPO pairs could be detected simultaneously in the SPL state, and a systematic shift away from disc dominated flux with the increasing power-law flux is detected as the HFQPO pairs shift from 276 to 184 Hz for XTE J1550-564 and from 450 to 300 Hz for GRO J1655-40 as shown in Figs. 5 and 7 of R02, respectively. In addition, Remillard (2004) noted that the broad Fe K emission lines can be also detected in the SPL state in XTE J1550-564 and GRO J1655-40. These results imply that the Fe K lines could be detected simultaneously with the 3:2 HFQPO pairs in these two sources.

In this paper, we interpret the 3:2 HFQPO pairs associated with the broad Fe K line in XTE J1550-564 and GRO J1655-40 by modifying MC-I model in two aspects. (1) The open field lines corresponding to the BZ process is removed, and (2) a non-zero torque exerted at the inner edge of the disc is introduced. Henceforth the modified model is referred to as MC-II model. It turns out that the 3:2 HFQPO pairs observed in the two sources can be fitted by tuning several model parameters, such as the BH spin, and the main features of MC-II model lie in the following aspects: (1) The condition for only one HFQPO is discussed based on the two mechanisms for producing the 3:2 HFQPO pairs. (2) An explanation is given for a systematic shift away from disc dominated flux with the increasing power-law flux as the HFQPO pairs shift from the higher to lower frequencies, which is consistent with the analysis given by R02. (3) The BH spin in XTE J1550-564 and GRO J1655-40 can be estimated by combining the 3:2 HFQPO pairs with the very steep emissivity index required for fitting the broad Fe K emission line.

This paper is organized as follows. In §2 we present a detailed description of MC-II model, in which the main differences between MC-I and MC-II models are outlined. In §3 we describe the elements for fitting the 3:2 HFQPO pairs observed in XTE J1550-564 and GRO J1655-40, and present the calculation sequence and results based on MC-II model. We discuss the possible correlation of the 3:2 HFQPO pairs with the very steep emissivity index required by broad Fe K α lines. It is expected that the 3:2 HFQPO pairs could be observed with the steep emissivity index, and the black hole spin could be estimated once the value ranges of the index are determined in the future observations. Finally, we discuss some issues related to MC-II model in §4.

Throughout this paper the geometric units $G = c = 1$ are used.

2 DESCRIPTION OF MC-II MODEL

In this section we present a detailed description of MC-II model based on the following assumptions.

(1) The accretion disc is perfectly conducting, and the closed magnetic field lines are frozen in the disc. The disc is thin and relativistic, lying in the equatorial plane of a Kerr black hole.

(2) Corona is introduced, which consists of tenuous hot plasma above the disc surface as shown in Figure 1. Both large- and small-scale magnetic fields are involved in MC-II model, in which the large-scale magnetic field plays a key role in transferring energy and angular momentum from a fast-rotating black hole to its surrounding disc in the MC process, while the small-scale

magnetic field energizes the corona above the disc by virtue of some physical processes, such as magnetic reconnection and buoyancy (Haardt & Maraschi 1991). It has been shown that the existence of corona can improve the fitting of the output spectra from the BHXBs, which is helpful to interpret the X-ray radiation observed in the SPL state (Ma et al. 2006).

(3) The large-scale magnetic field is assumed to be non-axisymmetric as described by Wang et al. (2003b, hereafter W03b). In addition, the magnetic field is assumed to be constant on the black hole horizon, and it varies as a power law with disc radius, i.e., $B_D \propto r^{-n}$.

(4) One of the main differences between MC-I and MC-II models lies in the fact that “no torque boundary condition” is assumed in MC-I model as given in SAD (Novikov & Thorne 1973, hereafter NT73; Page & Thorne 1974), while a nonzero torque is exerted at the inner edge of the disc in MC-II model. This torque arises from the magnetic connection of the matter in the plunging region with the matter in the inner disc as argued by some authors (Livio, Ogilvie & Pringle 1999, hereafter L99; Krolik 1999; Gammie 1999; Agol & Krolik 2000).

(5) Another difference between the two models lies in the fact that the open field lines are removed from MC-II model, while the closed field lines connecting the black hole with its surrounding accretion disc are retained, as shown in Figure 1. So only the MC process rather than the BZ process can work in MC-II model.

The reason for the modification of the magnetic field configurations lies in two points.

(i) The existence of the closed field lines depends upon the mapping relation with the conservation of the magnetic flux as argued in W03a, being not the sufficient condition for the existence of the open field lines at the horizon.

(ii) The second reason is more important, i.e., the 3:2 HFQPO pairs are observed in the SPL state, in which no jets are observed. Thus the magnetic field configuration depicted in Figure 1 is more consistent with the observations.

In order to illustrate the elements for interpreting the 3:2 HFQPO pairs we derive the radiation flux from the accretion disc based on MC-II model. According to the conservation of energy and angular momentum we have the following relations given in L02 and W03a,

$$\begin{cases} \frac{d}{dr}(\dot{M}_D L^\dagger - g_{vis}) = 4\pi r(F_{total} L^\dagger - H_{MC}), \\ \frac{d}{dr}(\dot{M}_D E^\dagger - g_{vis} \Omega_D) = 4\pi r(F_{total} E^\dagger - H_{MC} \Omega_D). \end{cases} \quad (1)$$

In equation (1) \dot{M}_D is the accretion rate. The quantities g_{vis} and H_{MC} are respectively the interior viscous torque in the disc and the flux of angular momentum transferred between the black hole and the disc in the MC process, and E^\dagger and L^\dagger are the specific energy and angular momentum of the disc matter, being given in NT73 as follows (where $\chi \equiv \sqrt{r/M}$),

$$E^\dagger = (1 - 2\chi^{-2} + a_* \chi^{-3}) / (1 - 3\chi^{-2} + 2a_* \chi^{-3})^{1/2}, \quad (2)$$

$$L^\dagger = M\chi(1 - 2a_* \chi^{-3} + a_*^2 \chi^{-4}) / (1 - 3\chi^{-2} + 2a_* \chi^{-3})^{1/2}. \quad (3)$$

By resolving equation (1) we derive the total radiation flux F_{total} and the interior viscous torque g_{vis} in the disc as follows,

$$F_{total} = F_{DA} + F_{MC} + F_{gin}, \quad (4)$$

$$g_{vis} = \frac{E^\dagger - \Omega_D L^\dagger}{-d\Omega_D/dr} 4\pi r F_{total}. \quad (5)$$

In equation (4) F_{DA} and F_{MC} are respectively the radiation fluxes contributed by the disc accretion and the MC process, and F_{gin} is the extra contribution due to the exterior torque exerted at the inner edge, and Ω_D is the angular velocity of the relativistic thin disc and it reads

$$\Omega_D = \frac{1}{M(\chi^3 + a_*)}. \quad (6)$$

In equation (6) the parameter $a_* \equiv J/M^2$ is the black hole spin, which is defined in terms of the black hole mass M and angular momentum J , and the parameter χ is related to the disc radius by $\chi = \sqrt{\xi} \chi_{ms}$, where $\xi \equiv r/r_{ms}$ is defined in terms of the innermost stable circular orbit (ISCO, NT73). The three parts of F_{total} are expressed as follows,

$$F_{DA} = \frac{1}{4\pi r} \frac{-d\Omega_D/dr}{(E^\dagger - \Omega_D L^\dagger)^2} \int_{r_{in}}^r (E^\dagger - \Omega_D L^\dagger) (\dot{M}_D dL^\dagger/dr) dr, \quad (7)$$

$$F_{MC} = -\frac{d\Omega_D}{r dr} (E^\dagger - \Omega_D L^\dagger)^{-2} \int_{r_{ms}}^r (E^\dagger - \Omega_D L^\dagger) H_{MC} r dr, \quad (8)$$

$$F_{gin} = \frac{1}{4\pi r} \frac{-d\Omega_D/dr}{(E^\dagger - \Omega_D L^\dagger)^2} \cdot g_{in} (E_{in}^\dagger - \Omega_{in} L_{in}^\dagger), \quad (9)$$

where $\Omega_{in} = \Omega_D(r_{in})$ is the angular velocity at r_{in} , other terms with subscripts “in” are taken their values at r_{in} .

The function H_{MC} in equation (8) is related to the MC torque by $\partial T_{MC}^{NA}/\partial r = 4\pi r H_{MC}$, and T_{MC}^{NA} is the MC torque due to non-axisymmetric magnetic field and it reads (W03b)

$$T_{MC}^{NA} = \lambda T_{MC}^A, \quad (10)$$

where T_{MC}^A is the MC torque due to axisymmetric magnetic field, being expressed in W03a as

$$T_{MC}^A/T_0 = 4a_* (1+q) \int_{\theta_S}^{\theta} \frac{(1-\beta_\Omega) \sin^3 \theta d\theta}{2 - (1-q) \sin^2 \theta}, \quad \theta_S < \theta < \theta_L. \quad (11)$$

The parameter λ in equation (10) is used to indicate the difference between T_{MC}^A and T_{MC}^{NA} as described in W03b, and $\beta_\Omega \equiv \Omega_D/\Omega_H$ is the ratio of the angular velocity of the disc to that of the black hole. It is easy to check by using equation (6) that $\beta_\Omega < 1$ always holds for a fast-spinning black hole with $a_* > 0.3594$, implying that energy and angular momentum are transferred from the black hole to the inner disc in the MC process.

Since the magnetic field on the black hole is supported by the surrounding disc, there is some relation between B_H and \dot{M}_D . One possibility has been suggested by Moderski et al. (1997), which is based upon the balance between the pressure of the magnetic field on the horizon and the ram pressure of the innermost parts of an accretion flow, i.e.,

$$B_H^2/(8\pi) = P_{ram} \sim \rho c^2 \sim \dot{M}_D/(4\pi r_H^2), \quad (12)$$

where r_H is the radius of the black hole horizon. Considering that equation (12) is not a certain relation between B_H and \dot{M}_D , we rewrite it as follows,

$$\dot{M}_D = \alpha_m B_H^2 r_H^2, \quad (13)$$

where α_m is a parameter to adjust the accretion rate \dot{M}_D .

Inspecting equation (9), we find that the contribution F_{gin} is related directly to the exterior torque g_{in} . According to L99 the strength of the magnetic field produced by dynamo process in the disc is given by

$$\frac{B_{dyn}^2}{4\pi} \sim \frac{W}{2h_{in}} = w_\varphi^r, \quad (14)$$

and the torque g_{in} is related to the viscous stress w_φ^r at r_{in} as follows,

$$g_{in} = r_{in} \cdot 2\pi r_{in} \cdot 2h_{in} \cdot w_\varphi^r, \quad (15)$$

where h_{in} is the half-thickness at r_{in} , being related to r_{in} by $h_{in} = \alpha_H r_{in}$.

In equation (14) W is the integrated shear stress of the disc, and the disc magnetic field B_D is related to B_{dyn} by

$$B_D \sim (h/r)_{\max} B_{dyn}, \quad (16)$$

where h is the half-thickness of the disc. As argued in W03a, the field B_D is related to B_H by

$$B_D = B_H (r_H/\varpi_{in}), \quad (17)$$

where ϖ_{in} is the cylindrical radius at r_{in} in the context of Kerr metric.

Incorporating equations (16) and (17), we have

$$B_{dyn}^2 = (r_{in}/h_{in})^2 B_D^2 = [(r_{in}r_H)/(\varpi_{in}h_{in})]^2 B_H^2. \quad (18)$$

Incorporating equations (14), (15) and (18), we have the torque g_{in} as follows,

$$g_{in} = \alpha_H B_{dyn}^2 r_{in}^3 = \alpha_H^{-1} r_{in}^3 (r_H/\varpi_{in})^2 B_H^2. \quad (19)$$

Assume that the inner edge of the disc is initially located at ISCO. If the magnetic pressure inside ISCO is strong enough, a radial force can be exerted at the inner edge of the disc due to the magnetic connection, resulting in an outward displacement of the inner edge from r_{ms} to r_{in} . It is assumed that the magnetic torque g_{in} exerted at r_{in} is determined by the following equations,

$$\delta g_{in} \Omega_{in} = [E^\dagger(r_{in}, a_*) - E^\dagger(r_{ms}, a_*)] \dot{M}_D, \quad (20)$$

where $g_{in} \Omega_{in}$ is the power of the magnetic torque, and δ is the fraction of the power keeping the inner edge at r_{in} .

3 FITTING 3:2 HFQPO PAIRS ASSOCIATED WITH BROAD FE K LINE

Considering the fact that the accretion disc is perfectly conducting, and the closed magnetic field lines are frozen in the disc, and the inner and outer hotspots are produced by non-axisymmetric magnetic field, we infer that these hotspots rotate with the angular velocity of the disc, and the upper and lower frequencies of the 3:2 HFQPO pairs can be expressed by

$$\nu_{HFQPO} = \nu_0 (\xi^{3/2} \chi_{ms}^3 + a_*)^{-1}, \quad (21)$$

where $\nu_0 \equiv (m_{BH})^{-1} \times 3.23 \times 10^4 \text{ Hz}$, and $m_{BH} \equiv M/M_\odot$ is the black hole mass in terms of one solar mass. Equation (21) can be derived directly from equation (6).

The lower frequency ν_{lower} of the HFQPO pair is produced by the outer hotspot, which is located at the outer boundary of the MC region as shown in Figure 1. According to the Kruskal-Shafranov criterion, the screw instability of the large-scale magnetic field will occur, if the magnetic field line turns around itself about once (Kadomtsev 1966; Bateman 1978). Based on the Kruskal-Shafranov criterion the radius r_{out} can be determined by the following equation (Wang et al. 2004),

$$(2\pi\varpi_D/L) B_D^p / B_D^T \leq 1, \quad (22)$$

where B_D^p and B_D^T are the poloidal and toroidal components of the magnetic field on the disc, respectively. The quantities L and ϖ_D are respectively the poloidal length of the field line and the cylindrical radius on the disc, and the latter reads

$$\varpi_D = \Sigma_D / \rho_D = \xi M \chi_{ms}^2 \sqrt{1 + a_*^2 \xi^{-2} \chi_{ms}^{-4} + 2a_*^2 \xi^{-3} \chi_{ms}^{-6}}, \quad (23)$$

where Σ_D and ρ_D are the Kerr metric parameters (Novikov & Thorns 1973).

Wang et al. (2004) expressed equation (22) in terms of the parameters involved in the MC process as follows,

$$(2\pi\varpi_D/L) F_{SC}(a_*, \xi, n) \leq 1. \quad (24)$$

The equality in equation (24) corresponds to the screw instability, and $F_{SC}(a_*, \xi, n)$ is a function of the parameters, a_* , ξ and n , and it reads

$$F_{SC}(a_*, \xi, n) = \frac{\xi^{1-n} (1+q) [2 \csc^2 \theta - (1-q)]}{2a_* (1-\beta_\Omega)} \sqrt{\frac{1 + a_*^2 \chi_{ms}^{-4} \xi^{-2} + 2a_*^2 \chi_{ms}^{-6} \xi^{-3}}{1 + a_*^2 \chi_{ms}^{-4} + 2a_*^2 \chi_{ms}^{-6}}}, \quad (25)$$

where $q \equiv \sqrt{1 - a_*^2}$ is a function of the black hole spin. Thus the position of the outer hotspot can be determined by the criterion (24) for the given a_* and n .

The upper frequency ν_{higher} of the HFQPO pair is produced by the inner hotspot, of which the position is determined by the maximum of the following function,

$$F_{HFQPO} \equiv \xi^2 F_{total} / F_0, \quad (26)$$

where $F_0 \equiv B_H^2 = B_8^2 \times (3 \times 10^{26} \text{ erg} \cdot \text{s}^{-1} \cdot \text{cm}^{-2})$ is defined as a unit of the radiation flux, and B_8 is the magnetic field in terms of 10^8 gauss .

The emissivity index can be calculated from the total radiation flux F_{total} based on the definition as follows,

$$\beta = -d \ln F_{total} / d \ln r. \quad (27)$$

Incorporating equations (4), (7), (8), (9), (19) and (27), we obtain the emissivity index $\beta = \beta_{DA} + \beta_{MC} + \beta_{gin}$ by calculating the following contributions,

$$\beta_{DA} \equiv -\frac{r}{F_{total}} \frac{dF_{DA}}{dr}, \quad \beta_{MC} \equiv -\frac{r}{F_{total}} \frac{dF_{MC}}{dr}, \quad \beta_{gin} \equiv -\frac{r}{F_{total}} \frac{dF_{gin}}{dr}, \quad (28)$$

where β_{DA} , β_{MC} and β_{gin} are contributed by the disc accretion, the MC process and the magnetic torque exerted at the inner edge of the disc, respectively.

Based on equations (7), (8), (9) and (28) we obtain the curves of the above contributions to the total radiation flux and the emissivity index versus the disc radius for XTE J1550-564 with $m_{BH} = 10.8$ as shown in Figure 2a and 2b, respectively.

As shown in Figure 2 the contributions of the disc accretion and the MC process to the total radiation flux and the emissivity index are more than two orders of magnitude less than those due to the magnetic torque at the inner edge of the disc, and both the total radiation flux F_{total} and the emissivity index β take their maxima at r_{in} . Thus we infer that both the inner hotspot and the maximum emissivity index are located at r_{in} .

Combining equation (21) with the higher and lower HFQPO frequencies corresponding to the disc radii $r_{in} = \xi_{in} r_{ms}$ and $r_{out} = \xi_{out} r_{ms}$, we have

$$\nu_{higher} = \nu_0 (\xi_{in}^{3/2} \chi_{ms}^3 + a_*)^{-1} \quad (29)$$

$$\nu_{lower} = \nu_0 (\xi_{out}^{3/2} \chi_{ms}^3 + a_*)^{-1} \quad (30)$$

Equations (20), (24), (27), (29) and (30) can be regarded as a set of equations for calculating the disc radii, r_{in} and r_{out} , for the 3:2 HFQPO pairs, and henceforth *the five independent equations* are referred to as **FIE**. Four input parameters, a_* , m_{BH} , ν_{higher} and ν_{lower} , are involved, and five output parameters, n , r_{in} , r_{out} , δ and β are obtained based on **FIE**. The detailed calculation sequence is described as follows.

(1) As the first step, we assume a value of spin with the observed black hole mass, e.g., $a_* = 0.5$ and $m_{BH} = 10.8$ for XTE J1550-564. Based on the higher frequency ν_{higher} , e.g., 276Hz for XTE J1550-564, the position of the inner hotspot can be determined by equation (29). Thus the radius r_{in} can be determined for the given black hole spin and mass.

(2) In the second step, the position of the outer hotspot corresponding to the lower frequency ν_{lower} , e.g., 184Hz for XTE J1550-564, can be determined by combining equation (30) with the criterion of the screw instability given by equations (24),

and the power law index n indicating the variation of the magnetic field with the disc radius can be determined in calculating ν_{lower} by virtue of the criterion of the screw instability.

(3) Finally, in the third step, the outward displacement of the inner edge from r_{ms} to r_{in} can be worked out, and the parameter δ is determined by equation (20). Combining equation (27) with equation (4) and the obtained values a_* , r_{in} and n , we have a maximum value of the emissivity index β located at r_{in} .

In this way, we can obtain one set of solution of r_{in} , r_{out} , n , δ and β by inputting each black hole spin a_* with the observed ν_{higher} , ν_{lower} and m_{BH} into **FIE**, and the curves of β , n and δ varying with a_* for XTE J1550-564 and GRO J1655-40 are shown in Figures 3 and 4, respectively.

By resolving **FIE** we have the specific solutions corresponding to the two BHBs with the lower and higher black hole masses and different spins as listed in Table 1.

Inspecting Figures 3 and 4, and Table 1, we find that the 3:2 HFQPO pairs observed in XTE J1550-564 and GRO J1655-40 can be worked out with the steep emissivity index, and the features of MC-II model are summarized as follows.

(1) For a given black hole mass, a bigger spin corresponds to a smaller emissivity index β and a smaller parameter n , but to a bigger parameter δ . For a given black hole spin, a bigger black hole mass corresponds to a bigger β , while the parameters n and δ are insensitive to the variation of the black hole mass. This result can be understood based on black hole physics (Shapiro & Teukolsky 1983). The width of the plunging region decreases monotonically with the increasing black hole spin, so the effects of the magnetic torque in the plunging region decreases with the increasing black hole spin.

(2) The black hole spin could be estimated, if the value range of the emissivity index can be determined by the future observations. As shown by the shaded regions in Figures 3a and 4a, the black hole spin could be constrained in the range of $0.7 < a_* < 0.998$ with the emissivity indexes in the ranges of $3.95 < \beta < 4.12$ and $3.95 < \beta < 4.24$ for XTE J1650-564 and GRO J1655-40, respectively.

As pointed out in RM06, HFQPOs are likely to offer the most reliable measurement of BH spins once the correct model is known. The observations involved HFQPOs are very complicated, behaving multiple features in different sources, and a variety of mechanisms and models are invoked to fit the HFQPOs in BHBs. The model of the MC process with a nonzero torque exerted at the inner edge of accretion disc provides an interpretation for the association of the 3:2 HFQPO pairs with the broad Fe K line, and it could be a possible approach to the BH spins of the binaries in the Galaxy.

4 DISCUSSION

In this paper, association of the 3:2 HFQPO pairs with the broad Fe K line in XTE J1550-564 and GRO J1655-40 is discussed based on MC-II model. It is shown that the 3:2 HFQPO pairs observed in the two sources can be fitted with the observational constraints by tuning several model parameters. Some related issues are given as follows.

(1) It is noted that the mechanisms of creating the two hotspots are different: the inner one is produced predominantly by the magnetic torque exerted at the inner edge of the disc, while the outer one arises from the screw instability of the large-scale magnetic field. It is helpful to imagine the magnetic field line as an elastic string. The rotating BH twists the field line, while the field line tries to untwist itself. Once the toroidal component of the magnetic field is strong enough to satisfy the criterion, the screw instability will occurs, just as a twisted elastic string releases its energy under appropriate conditions.

(2) Some authors argued that the coronal heating in some stars including the Sun is probably related to dissipation of currents, and very strong X-ray emissions arise from variation of magnetic fields (Galsgaard & Parnell 2004; Peter et al. 2004). Analogously, if the corona exists above the disc in MC-II model, we expect that the corona above r_{out} might be heated by the induced current due to the screw instability of the non-axisymmetric magnetic field. Thus the ratio of the disc bolometric flux to the power-law flux is greater for the inner hotspot than that for the outer hotspot, and the feature of X-ray radiation given by R02 can be interpreted based on MC-II model with corona, i.e., there exists a systematic shift away from disc dominated flux with the increasing power-law flux as the HFQPO pairs shift from the higher frequency to the lower frequency based on the observations of XTE J1550-564 and GRO J1655-40.

(3) Since the two hotspots are produced by two different mechanisms, we can explain the observations that HFQPOs do not always appear in simultaneous pairs, because the condition for the magnetic torque and that for the screw instability would not be satisfied at the same time. Since the inner and outer hotspots are related to two different mechanisms based on the non-axisymmetric magnetic fields in the plunging region and the BH horizon, either the fluctuations of the magnetic fields at different position or the criterion of the screw instability could affect the HFQPO pairs. Unfortunately, we cannot discuss this issue in a quantitative way due to the unknown origin of the magnetic field near the BH.

(4) According to equation (21) the HFQPO frequency is inversely proportional to the BH mass, which provides a strong limit to the fits. We can neither fit the HFQPO with 92 Hz in XTE J1550-564 nor the 3:2 HFQPO pair (67, 41Hz) in GRS 1915+105 based on equation (21) for the measured BH masses. Furthermore, the 3:2 HFQPO pair (168, 113Hz) of GRS 1915+105 are not fitted, because a systematic shift away from disc dominated flux with the increasing power-law flux as the HFQPO pair shift from the higher frequency to the lower frequency has not been observed in this source.

(5) As argued above, the higher and lower HFQPO frequencies are related to the inner and outer hotspots rotating with the angular velocity located at r_{in} and r_{out} , respectively. According to equation (21) the HFQPO frequencies are inversely proportional to the BH mass, and the spin is related to the HFQPO frequencies via r_{in} and r_{out} , where the HFQPO frequencies are calculated by the angular velocity. Since the evolution time scale of the BH mass and spin are much longer than the observation time scale, the two quantities are considered fixed in calculations.

(6) As pointed out in R02, the 3:2 HFQPO pairs could have a small, but significant, change in frequency. For example, the HFQPO frequencies observed in XTE J1550-564 deviate from 274 Hz and 184 Hz during different outbursts. These small deviations in HFQPO frequencies can be calculated by resolving **FIE** with the adjustable parameters n and δ as shown in Table 2.

(7) As argued above, both the non-axisymmetric magnetic field configuration and the corona above the disc surface are required for interpreting the 3:2 HFQPO pairs observed in the SPL state of the BHXBs. Thus we can interpret the observation that sometimes the 3:2 HFQPO pairs cannot be observed in the SPL state, if the magnetic field configuration is axisymmetric. Based on the same reason we predict that the 3:2 HFQPO pairs could be observed with the very steep emissivity index, if the magnetic field configuration is non-axisymmetric. However, the HFQPO pairs cannot be produced with the emissivity index for the axisymmetric magnetic field configuration.

(8) According to $B_D \propto r^{-n}$ the ratio of the magnetic field at r_{out} to that at r_{in} can be written as $R_B \equiv (B_D)_{out}/(B_D)_{in} = (r_{in}/r_{out})^n$. Based on **FIE** we have the curves of R_B for XTE J1650-564 vary with a_* as shown in Figure 5, from which a strongly constraint to the BH spin can be found. The BH spin should be very high, or at least greater than some intermediate value to avoid the magnetic field at r_{out} too low to produce an outer hotspot.

(9) There is less certain evidence that the same 3:2 ratio occurs for QPOs observed in low-mass active galactic nuclei, Sgr A*, (Török 2005a, b; Ashenbach 2004a, b) and in a few nearby Seyferts (Lachowicz et al. 2006). MC-II model can be used to fit QPOs pairs observed in the super-massive BH systems, and we obtain the curves of the emissivity index β , the power-law index n and the parameter δ varying with the BH spin of for Sgr A* as shown in Figure 6.

We can find from Figure 6 that the parameter n varies from 4.272 to 7.108 with a_* decreasing from 0.998 to 0.853 for $m_{BH} = 4.4 \times 10^6$, while it varies from 5.040 to 10.239 with a_* decreasing from 0.998 to 0.555 for $m_{BH} = 2.6 \times 10^6$.

(10) The parameter n is used to indicate the variation of the large-scale magnetic field with the disc radius, which is a key parameter for fitting the 3:2 frequency ratio. Based on **FIE** we have the variation of the 3:2 frequency ratio with the parameter n for the given values of the BH spin as shown in Figure 7.

Inspecting Figure 7, we find that the frequency ratio decreases monotonically with the increasing parameter n . The greater n corresponds to the less ratio for the given spin, and the greater spin corresponds to both the less value and less variation of n for the given ratio. For XTE J1550-564, e.g., the ratio increases about 5.7% as the value of n decreases about 10% for $a_* = 0.5$, while the same variation occurs as n only decreases about 1.9% for $a_* = 0.998$. This result implies that the observed 3:2 frequency ratio is reached for a very narrow range of n with the greater BH spin.

(11) Finally, we discuss the values of the parameters α_H and α_m , which are used to indicate the disc thickness at r_{in} and the strength of the accretion rate, respectively. The emissivity index of XTE J1550-564 varies with the BH spin for different values of α_H and α_m are shown in Figure 8.

Inspecting Figure 8a, we find that the values of the emissivity index are insensitive to the values of α_H and α_m , provided that they are limited to $\alpha_H \leq 0.1$ and $\alpha_m \leq 1.0$. These value ranges are reasonable for thin accretion disc in MC-II model. In addition, based on the features of MC-II model, the 3:2 HFQPO pairs are also insensitive to the parameters with the above limited values.

Acknowledgements: This work is supported by the National Natural Science Foundation of China under grant 10873005 and National Basic Research Program of China under grant 2009CB824800. We are grateful to the anonymous referee for his (her) helpful comments on the manuscript.

REFERENCES

- Abramowicz, M. A., & Kluzniak, W. 2001, *A&A*, 374, L19
 Abramowicz, M. A., Karas, V., Kluzniak, W., & Lee, W. H., Rebusco, P., 2003, *PASJ*, 55, 467
 Agol, E., & Krolik, J. H., 2000, *ApJ*, 528, 161
 Aschenbach, B., et al. 2004a, *A&A*, 417, 71
 —. 2004b, *A&A*, 425, 1075
 Bateman G. *MHD Instabilities*, 1978, (Cambridge: The MIT Press)
 Blandford, R. D., & Znajek, R. L. 1977, *MNRAS*, 179, 433
 Blandford, R. D., 1999, in *ASP Conf. Ser. 160, Astrophysical Discs: An EC Summer School*, ed. . A. Sellwood & J. Goodman (San Francisco: ASP), 265
 Bradt, H. V., Rothschild, R. E., & Swank, J. H., 1993, *A&AS*, 97, 355
 Diaz Trigo, M., et al., 2007, *A&A*, 462, 657
 Galsgaard, K., & Parnell, C., *Proceedings of SOHO 15 Coronal Heating, ESA publication*, astro-ph/0409562
 Gammie, C. F., 1999, *ApJ*, 522, L57
 Haardt, F., & Maraschi, L., 1991, *ApJ*, 380, L51
 Kadomtsev B. B. 1966, *Rev. Plasma Phys.*, 2, 153
 Kluzniak, W., & Abramowicz, M. A., Lee, W., 2004, *AIPC* 714, 379
 Krolik, J. H., 1999, *ApJ*, 515, L73
 Lachowicz P., Czerny B. & Abramowicz M.A., 2006, astro-ph/0607594
 Li, L.-X., 2000, *ApJ*, 533, L115

- . 2002, *ApJ*, 567, 463 (L02)
- Livio M., Ogilvie G. I., Pringle J. E., 1999, *ApJ*, 512, 100 (L99)
- Ma, R.-Y., Wang, D.-X., & Zuo, X.-Q., 2006, *A&A*, 453, 1
- McClintock, J E, & Remillard R A 2006. In *Compact Stellar X-ray Sources*, ed. WHG Lewin, M van der Klis, pp. 157–214. Cambridge: Cambridge University Press. (astro-ph/0306213) (MR06)
- Miller, J. M. et al. 2001, *ApJ*, 563, 928
- Miller, J. M. et al., 2003, *MNRAS*, 338, 7
- Miller, J. M., et al., 2004. *ApJ*. 601, 450
- Miller, J. M., 2007, *ARA&A*, 45, 441
- Miniutti, G., Fabian, A. C., & Miller, J. M., 2004, *MNRAS*, 351, 466
- Moderaki, R., Sikora, M., Lasota, J. P. 1997, in *Ostrowski M., Sikora M., Madejski, G., Belgeman M., eds, Proc. International Conf., Relativistic Jets in AGNs. Krakow*, p. 110
- Novikov I. D., Thorne K. S., 1973, in *Dewitt C., ed., Black holes*. Gordon and Breach, New York (NT73)
- Page, D. N., & Thorne, K. S. 1974, *ApJ*, 191, 499
- Peter, H., Gudiksen, B., & Nordlund, A., 2004, *ApJ*, 617, L85
- Remillard, R. A., et al., Morgan, E. H., McClintock, J. E., Bailyn, C. D., & Orosz, J. A. 1999, *ApJ*, 522, 397
- Remillard, R. A., Munro, M. P., McClintock, J. E., & Orosz, J. A. 2002, *ApJ*, 580, 1030 (R02)
- Remillard, R. A. 2004, *AIPC*, 714, 13
- Remillard, R. A., & McClintock J. E. 2006, *ARA&A*, 44, 49 (RM06)
- Shapiro S. L., & Teukolsky S. A., 1983, *Black Holes, White Dwarfs and Neutron Stars*, John Wiley & Sons, Inc. New York
- Silbergleit, A. S., & Wagoner, R. V. 2007, arXiv:0711.4848
- Sobczak, G. J., et al., 2000, *ApJ*, 544, 993
- Strohmayer, T. E., 2001a, *ApJ*, 552, L49
- . 2001b, *ApJ*, 554, L169
- Török, G., 2005a, *Astron. Nachr.*, 326, 9, 856
- Török, G., 2005b, *A&A*, 440, 1
- Török, G., Abramowicz, M. A., Kluzniak, W., & Stuchlik, Z., 2005, *A&A*, 436, 1.
- van der Klis, M., 2000, *ARA&A*, 38, 717.
- van der Klis, M., 2006, In *Compact Stellar X-ray Sources*, ed. WHG Lewin, & M van der Klis, pp. 39 - 112. Cambridge, UK: Cambridge University Press. (astro-ph/0410551)
- Wagoner, R. V., Silbergleit, A. S., & Ortega-Rodriguez, M. 2001, *ApJ*, 559, L25
- Wang, D.-X., Xiao K., & Lei W.-H. 2002, *MNRAS*, 335, 655
- Wang, D.-X., Ma, R.-Y., Lei, W.-H., & Yao, G.-Z., 2003a, *ApJ*, 595, 109 (W03a)
- . 2003b, *MNRAS*, 344, 473 (W03b)
- . 2004, *ApJ*, 601, 1031
- Wang, D.-X., Ye, Y.-C., Yao, G.-Z., & Ma, R.-Y., , 2005, *MNRAS*, 359, 36
- Wilms J. et al. 2001, *MNRAS*, 328, L27

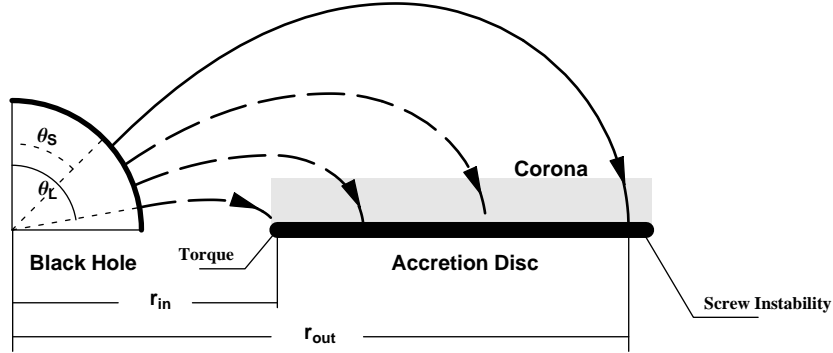


Figure 1. The Poloidal magnetic field configuration of MC-II model.

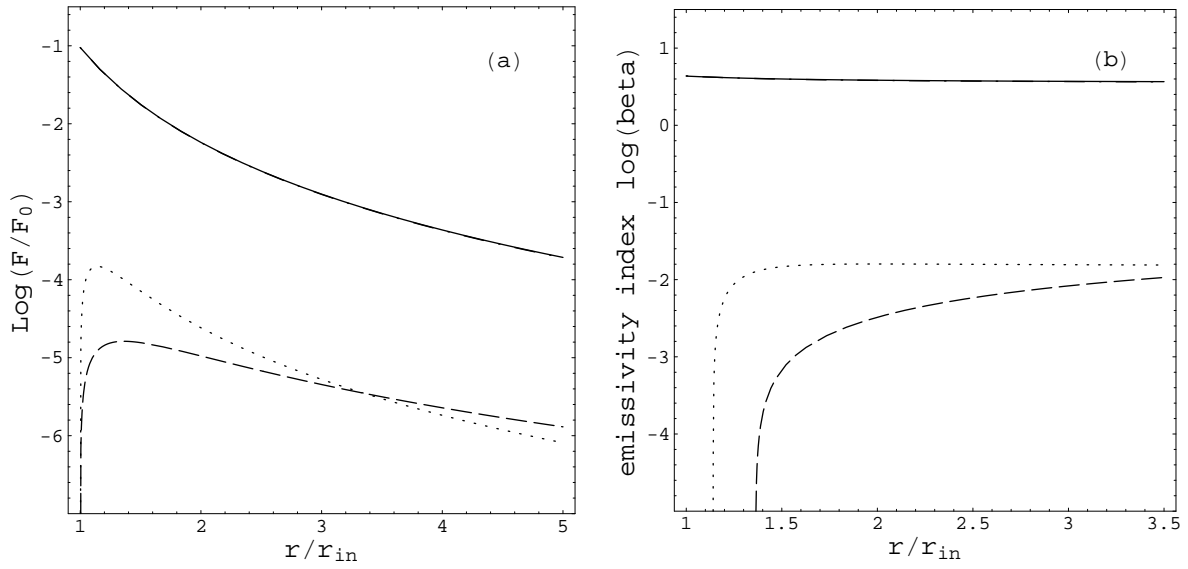


Figure 2. (a) Curves of $\log(F_{gin}/F_0)$, $\log(F_{DA}/F_0)$ and $\log(F_{MC}/F_0)$ versus r/r_{in} in solid, dashed and dotted lines, respectively. (b) Curves of $\log\beta_{gin}$, $\log\beta_{DA}$ and $\log\beta_{MC}$ versus r/r_{in} in solid, dashed and dotted lines, respectively. These curves are plotted for XTE J1550-564 with $m_{BH} = 10.8$, $a_* = 0.7$, $n = 9.99$ and $\delta = 3.29 \times 10^{-4}$.

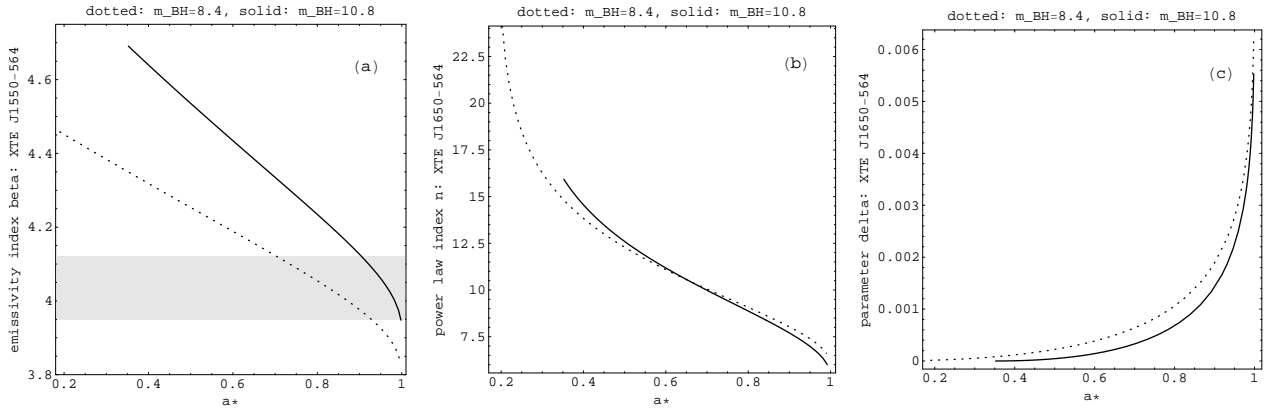


Figure 3. The curves of the emissivity index β , the power-law index n and the parameter δ versus the black hole spin a_* for XTE J1550-564 are shown in Figures 3a, 3b and 3c, respectively. The solid and dotted lines correspond to the upper and lower limits to the black hole mass, respectively. The shaded region in Fig. 3a indicates $3.95 < \beta < 4.12$.

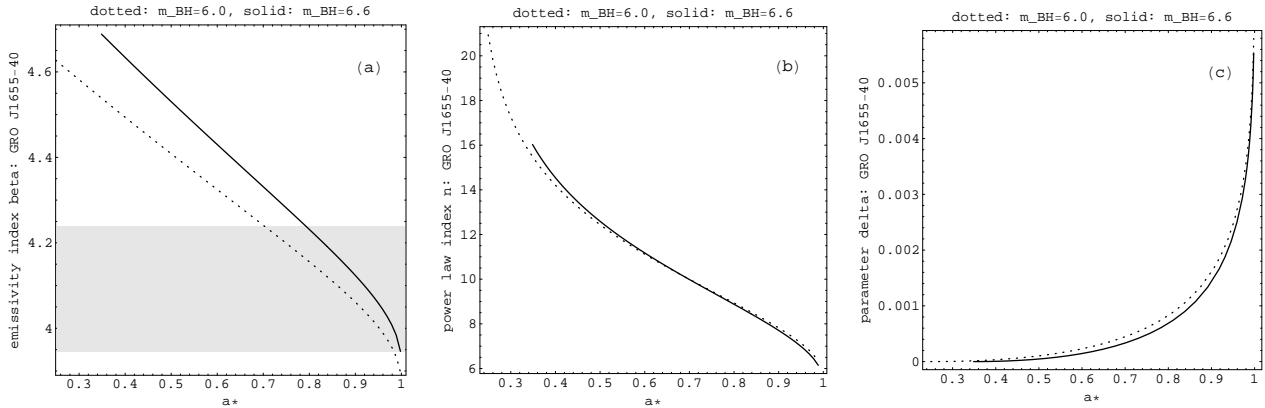


Figure 4. The corresponding curves for GRO J1655-40 with the same caption as given in Fig.3, except that the shaded region indicates $3.95 < \beta < 4.24$.

Table 1. Calculation results for the 3:2 HFQPO pairs and the emissivity index based on MC-II model.

Source	Input Quantities				Output Quantities		
	ν_{higher}	ν_{lower}	a_*	m_{BH}	n	δ	β
XTE J1550-564	276Hz	184Hz	0.5	8.4	12.29	2.22×10^{-4}	4.25
				10.8	12.60	4.42×10^{-5}	4.54
			0.7	8.4	10.05	6.37×10^{-4}	4.12
				10.8	9.99	3.29×10^{-4}	4.33
			0.998	8.4	6.23	6.22×10^{-3}	3.83
				10.8	5.65	5.52×10^{-3}	3.95
GRO J1655-40	450Hz	300Hz	0.5	6.0	12.44	1.03×10^{-4}	4.41
				6.6	12.59	4.60×10^{-5}	4.53
			0.7	6.0	9.99	4.45×10^{-4}	4.24
				6.6	9.99	3.33×10^{-4}	4.33
			0.998	6.0	5.87	5.79×10^{-3}	3.90
				6.6	5.66	5.53×10^{-3}	3.95

Notes: The input quantities of XTE J1550-564 and GRO J1655-40 are taken from RM06. The parameter δ is defined in equation (20) as the fraction of the power of the magnetic torque to keep the inner edge at r_{in} .

Table 2. Fits of the small changes in HFQPO frequency of XTE J1650-564 with $m_{BH} = 10.8$.

Source		1998-99A	1998-99B	2000 Apr 30-May 9
ν_{higher} (Hz)		281.7 ± 1.5	277.7	269.4 ± 2.7
ν_{lower} (Hz)		187.8	185.1 ± 3.5	178.6
Ratio		$1.5^{+0.01}_{-0.01}$	$1.5^{+0.03}_{-0.03}$	$1.5^{+0.02}_{-0.01}$
0.5	δ	$3.46^{+0.23}_{-0.24} \times 10^{-5}$	4.12×10^{-5}	$5.68^{+0.53}_{-0.56} \times 10^{-5}$
	n	$12.64^{+0.14}_{-0.14}$	$12.60^{+0.57}_{-0.52}$	$12.40^{+0.25}_{-0.27}$
	β	$4.565^{+0.008}_{-0.008}$	4.544	$4.502^{+0.014}_{-0.013}$
a_*	0.7	$3.06^{+0.06}_{-0.06} \times 10^{-4}$	3.22×10^{-4}	$3.57^{+0.12}_{-0.11} \times 10^{-4}$
	n	$9.99^{+0.10}_{-0.10}$	$9.98^{+0.39}_{-0.35}$	$9.88^{+0.18}_{-0.19}$
	β	$4.356^{+0.006}_{-0.005}$	4.341	$4.310^{+0.010}_{-0.009}$
0.998	δ	$5.47^{+0.01}_{-0.01} \times 10^{-3}$	5.51×10^{-3}	$5.59^{+0.04}_{-0.03} \times 10^{-3}$
	n	$5.61^{+0.02}_{-0.03}$	$5.64^{+0.05}_{-0.04}$	$5.69^{+0.04}_{-0.05}$
	β	$3.959^{+0.003}_{-0.003}$	3.951	$3.935^{+0.005}_{-0.005}$

Notes: (1) The super- and sub-scripts in δ , n and β correspond to up and down deviations of HFQPO frequencies, respectively. (2) The value of δ only depends on a_* and ν_{higher} , being independent of the deviation of ν_{lower} in the case of 1998-99B.

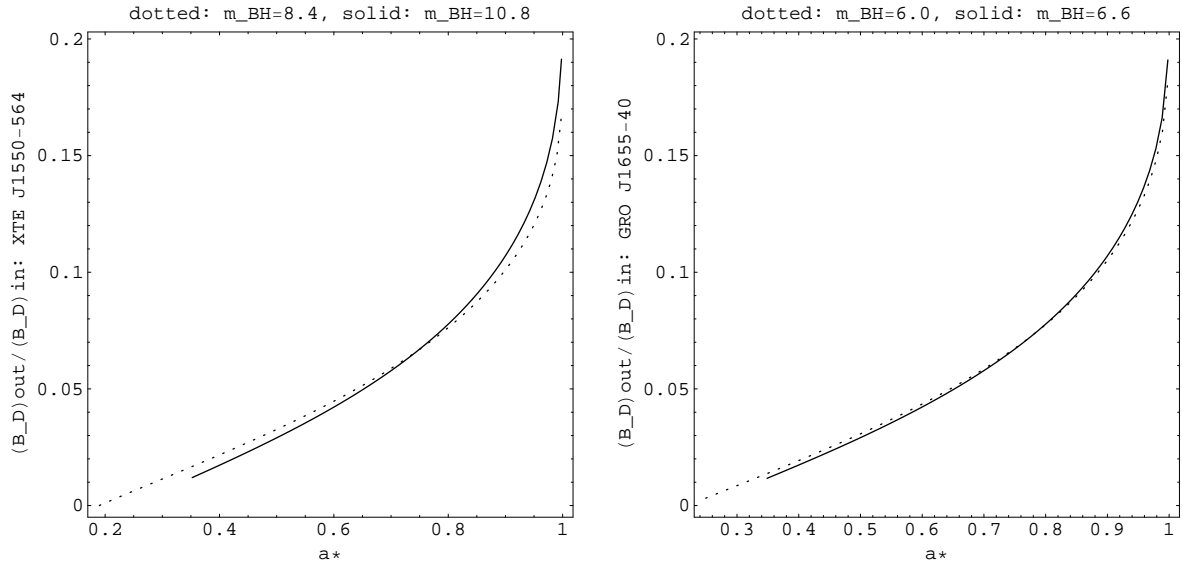


Figure 5. The curves of the ratio R_B versus the black hole spin a_* for (a) XTE J1550-564 and for (b) GRO J1655-40. The solid and dotted lines correspond to the higher and lower limits to the black hole mass, respectively.

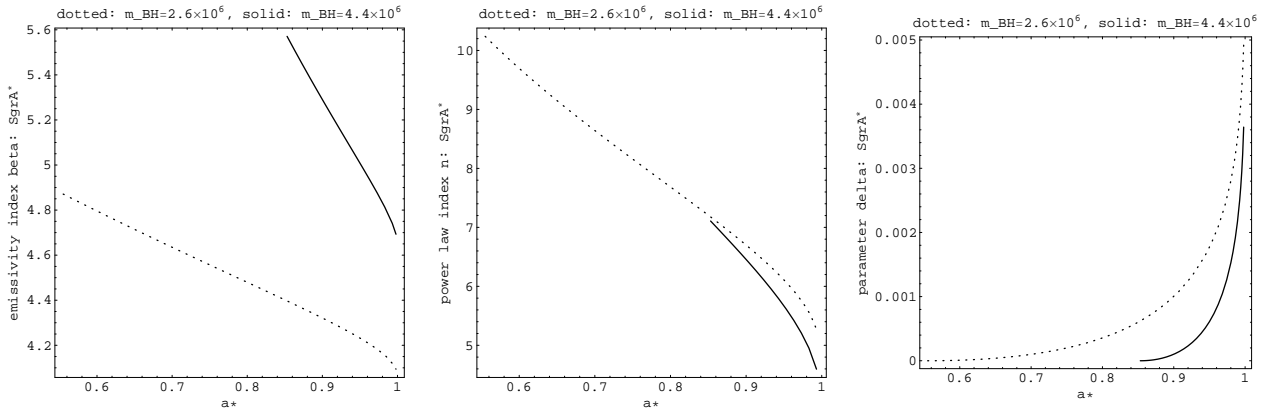


Figure 6. The curves of the emissivity index β , the power-law index n and the parameter δ versus the black hole spin a_* for Sgr A* are shown in Figures 6a, 6b and 6c, respectively. The solid and dotted lines correspond to the higher and lower limits to the black hole mass ($m_{BH} = 4.4 \times 10^6$ and $m_{BH} = 2.6 \times 10^6$).

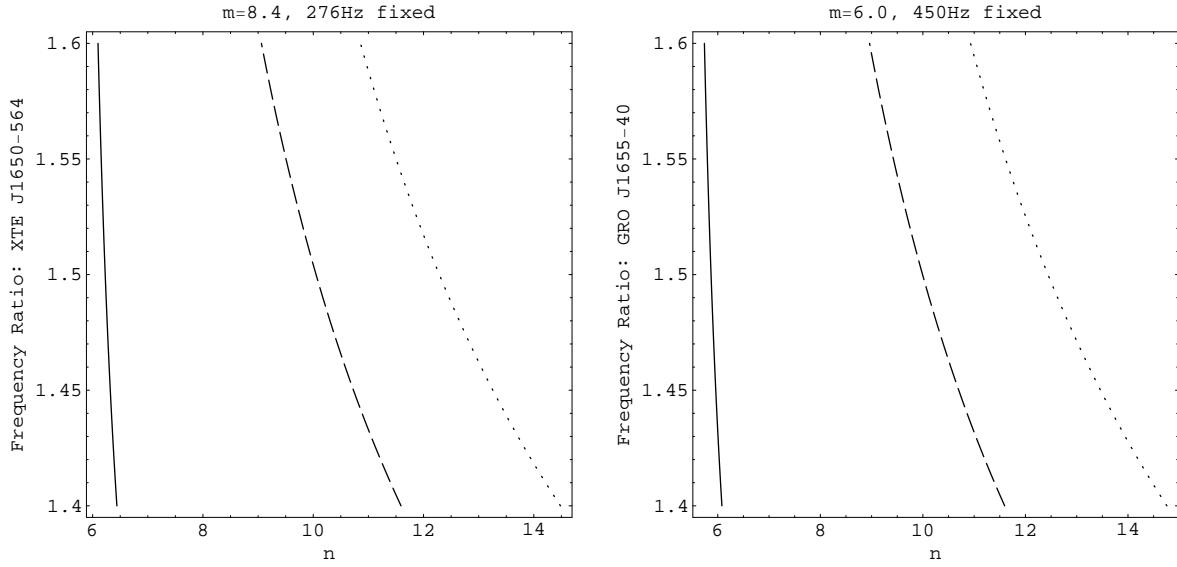


Figure 7. The variation of the frequency ratio with the parameter n for (a) XTE J1550-564 and for (b) GRO J1655-40. The solid, dashed and dotted lines correspond to $a_* = 0.998, 0.7$ and 0.5 , respectively.

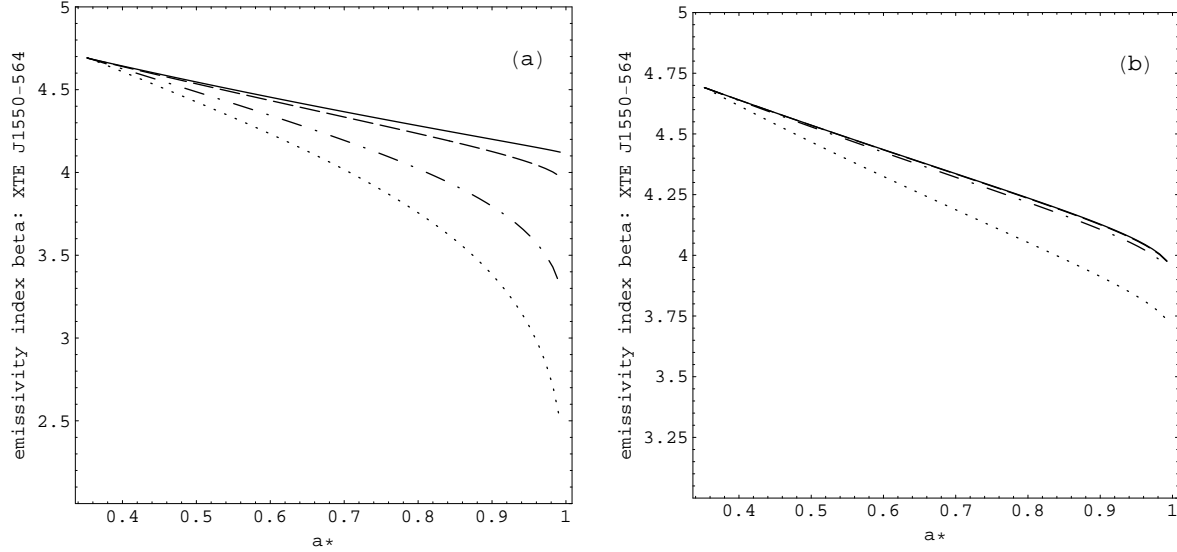


Figure 8. The curves of emissivity index of XTE J1550-564 versus the black hole spin for (a) $\alpha_m = 0.1$, and $\alpha_H = 0.01, 0.1, 0.5$ and 1.0 in solid, dashed, dot-dashed and dotted lines, respectively, and for (b) $\alpha_H = 0.1$, and $\alpha_m = 0.01, 0.1, 1.0$ and 10.0 in solid, dashed, dot-dashed and dotted lines, respectively. The black hole mass is taken as $m_{BH} = 10.8$.